Soft Matter

Static structure and dynamical behavior of colloidal liquid crystals consisting of hydroxyapatite-based nanorod hybrids

Journal:	*Soft Matter*
Manuscript ID	SM-ART-01-2019-000101.R1
Article Type:	Paper
Date Submitted by the Author:	14-Feb-2019
Complete List of Authors:	Hoshino, Taiki; RIKEN, SPring-8 Center Nakayama, Masanari; University of Tokyo, Department of Chemistry and Biochemistry Fujinami, So; RIKEN, SPring-8 Center Nakatani, Tomotaka; RIKEN, SPring-8 Center Kohmura, Yoshiki; RIKEN, SPring-8 Center Kato, Takashi; University of Tokyo, Chemistry and Biochemistry

Static structure and dynamical behavior of colloidal liquid crystals consisting of hydroxyapatite-based nanorod hybrids

Taiki Hoshino*[1], Masanari Nakayama[2], So Fujinami[1], Tomotaka Nakatani[1], Yoshiki Kohmura[1], Takashi Kato*[2]

[1]RIKEN, SPring-8 Center, 1-1-1 Kouto, Sayo-cho, Sayo-gun, Hyogo 679-5148, Japan,
[2] Department of Chemistry and Biotechnology, School of Engineering, The University of Tokyo, 7-3-1 Hongo, Bunkyo-ku, Tokyo 113-8656, Japan

Abstract

Biominerals such as bones and teeth have elaborated nanostructures composed of aligned anisotropic hydroxyapatite (HAp) nanocrystals, which results in high mechanical properties. Construction of such ordered structures of HAp nanocrystals is challenging in synthetic materials. Recently, we found that HAp-nanorods-based colloidal liquid crystals are obtained. In the present study, the static structure and dynamics of liquid-crystalline (LC) colloidal dispersions of HAp nanorods are investigated by small-angle X-ray scattering (SAXS) and X-ray photon correlation spectroscopy (XPCS). The SAXS results reveal that the interparticle distance decreases with increasing a certain HAp concentration, ϕ_{HAp}, and the decrease of the interparticle distance for the short-axis direction is significantly smaller in the LC phase than the interparticle distance in the isotropic phase. In the dynamical studies of the LC phase using XPCS, we observe the diffusive motion of the HAp colloids, with the diffusion coefficient being dependent on the wave number. The diffusive motion slows down with increasing ϕ_{HAp}. We observe anisotropic dynamics after long-term storage (160 days after sealing), whereas only isotropic dynamics are observed in the initial XPCS measurements after short-term storage (14 days after sealing). Moreover, we have found that the dynamics slows down with increasing storage time.

Introduction

In nature, biominerals such as bones and teeth have well-organized structures composed of anisotropic hydroxyapatite (HAp).[1,2] It is interesting to achieve such sophisticated assembled and hybrid structures of nanocrystals for development of new functional materials.[3,4,5] Recently, we reported new colloidal liquid crystals based on HAp nanorods, which form aligned films of HAp nanorods.[6] This liquid crystal is a biocompatible ordered material. Detailed analyses for the liquid-crystalline (LC) ordered structures and dynamics are important for control of the properties of these HAp-based hybrid materials.

Here we report the static structure and dynamics of colloidal LC dispersions of HAp nanorods investigated by small-angle X-ray scattering (SAXS) and X-ray photon correlation spectroscopy (XPCS). The evaluation of the correlation between the static structure and dynamics in a concentrated anisotropic particle dispersion system is described.

The static structure and dynamics of anisotropically shaped particles dispersed in a liquid provide important information as models of anisotropic systems such as polymers and viruses.[7,8] The diffusive behavior of rod-like particles has been investigated by various techniques such as time-resolved fluorescence video microscopy,[9.10,11] dynamic light scattering (DLS),[12] depolarized DLS, and multipolarization DLS.[13,14,15] Extensive numerical simulation studies have also been performed using Brownian dynamics, molecular dynamics,[16,17,18] and Monte Carlo methods.[19,20,21] In most of these experimental and simulation studies, the diffusion coefficients were evaluated separately in the long- and short-axis directions under various conditions, and in some of these studies, the rotational behavior was thoroughly discussed. Although the diffusion coefficients were evaluated as constant values in most of these studies, the diffusion coefficient in a concentrated dispersion system is not constant but depends on the wave number q, owing to the influence of interparticle correlation as has been discussed for spherical particles.[22,23,24,25,26,27,28] To observe such behavior in optically opaque samples, it is necessary to monitor the fluctuation of the particles for a sufficiently large range of q. X-ray scattering techniques are powerful tools owing to the high penetration depth of X-rays into materials. Information regarding the static structure and dynamics can be obtained by SAXS measurements and XPCS, respectively, two techniques with a very similar measured q range. The principle of XPCS is basically the same as that of DLS and this method permits the dynamics to be measured up to a relatively high q for concentrated particle dispersion systems using partially coherent X-rays. Several pioneering studies investigating the dynamics of anisotropic particles by XPCS have been performed. Holmqvist *et al*. investigated the dynamics of concentrated charged gibbsite platelets and successfully evaluated the rotational modes.[29] Wagner *et al*. investigated the diffusive motion of magnetic rod-like particles in an external magnetic field and discussed the dependence of the anisotropic diffusion coefficient on the aspect ratio.[30] In these studies, since the measured q range

was relatively narrow or a dilute dispersion was used, there was no need to consider the influence of interparticle correlation on the diffusion coefficient.

Experimental

Six aqueous HAp colloidal dispersions with different concentrations were prepared. These were obtained by mixing aqueous $CaCl_2$ and K_3PO_4 solutions in the presence of poly(acrylic acid) (PAA; $M_w = 2.0 \times 10^3$) as an additive; the preparation method was described in detail in the previous paper.[6] The colloidal particles produced by this method form nanorods consisting of HAp and PAA with a length of approximately 100 nm and a width of approximately 20 nm. The concentrations of HAp, ϕ_{HAp}, in the prepared dispersions were 3.8, 5.0, 6.3, 6.5, 7.5, and 8.7 vol %, and the concentrations combined with PAA were 5.6, 7.3, 9.2, 9.6, 11.0, and 12.7 vol %, respectively, as determined by thermogravimetric measurements. Polarized optical microscopy revealed that the dispersions existed as the isotropic phase at ϕ_{HAp} = 3.8, 5.0, and 6.3 vol % and as the LC phase (nematic phase) at ϕ_{HAp} = 6.5, 7.5, and 8.7 vol %. For the X-ray scattering measurements, the samples were sealed in 10-μm-thick quartz capillary tubes with a diameter of 2 mm. All of the X-ray scattering measurements were conducted at room temperature.

The SAXS measurements were performed on beamline BL05XU at SPring-8 (Hyogo, Japan). The undulator source and Si(111) monochromator were tuned to an energy of 8.00 keV, the X-ray beam was focused around the detector position, and higher harmonic X-rays were removed using Rh-coated mirrors. The scattered X-rays were detected using a PILATUS 1M detector (Dectris, Switzerland) mounted approximately 4.4 m downstream of the sample. To investigate the static structure change depending on the stationary period, the SAXS measurements were performed twice. The first measurements were conducted for short-term storage samples (15 days after sealing) and the second measurements were conducted for long-term storage samples (185 days after sealing).

The XPCS measurements were conducted on beamline BL29XUL at SPring-8.[31] The undulator source and Si(111) monochromator were tuned to an energy of 12.40 keV and higher harmonic X-rays were removed using Pt-coated mirrors. The sample was irradiated with partially coherent X-rays obtained by passing the beam through 20×20 μm^2 slits, and the scattered X-rays were detected using an EIGER 1M two-dimensional detector (Dectris, Switzerland) mounted approximately 5.4 m downstream of the sample. During the XPCS measurements, the fluctuation of the scattering intensity, $I(\mathbf{q},t)$, at a scattering vector $\mathbf{q}$ was obtained in a time series, t, and the intensity time autocorrelation function $g_2(q,t)$ was evaluated as

$$g_2(q,t) = \langle I(q,t')I(q,t'+t)\rangle / \langle I(q,t')\rangle^2, \quad (1)$$

where $q = |\mathbf{q}|$ and the angle brackets indicate time averaging. To investigate the change in dynamics due to the storage period, the XPCS measurements were performed for both short-term storage samples (14 days after sealing) and long-term storage samples (160 days after sealing). Since the relaxation of $g_2(q,t)$ in the isotropic phase was faster than the measurable time range, only the data for the LC phase is presented. For both the SAXS and XPCS measurements, data were acquired for multiple (10–20) irradiation positions within the range of 5 mm, all of which were located more than 5 mm from the bottom of the capillary tube. Since the irradiation position was found to have a negligible influence on the measurements, the data presented herein were obtained by averaging the measurements at multiple irradiation positions, except for the scattering images and profiles thereof. The error bars depicted in the subsequent graphs were obtained from the data deviations of those multiple measurements.

Results and discussion

Static structure

Figure 1 presents representative scattering data obtained from the short-term storage samples. The scattering image obtained from the sample with ϕ_{HAp} = 5.0 vol % is shown in Fig. 1(a). The isotropic pattern of the SAXS image indicates that the particles have no preferential orientation (Fig. 1(b)), and the q value of the ring-shaped peak corresponds to the average interparticle distance. Similar isotropic scattering images with shifts of the peak position were observed for the other two samples existing as isotropic phases with ϕ_{HAp} = 3.8 and 6.3 vol %. Figure 1(c) shows the circularly averaged intensity profile with respect to q obtained from Fig. 1(a), revealing a maximum at $q \approx 0.15\ \mathrm{nm}^{-1}$, and from this, the average interparticle distance was estimated as $d \approx 42\ \mathrm{nm}$.

The scattering image obtained from the sample with ϕ_{HAp} = 8.7 vol % is presented in Fig. 1(d). This image exhibits an anisotropic pattern due to the orientation of the particles (Fig. 1(e)), unlike the scattering images obtained for the isotropic phase. Considering the anisotropy of the particle shape, the directions $q_{//}$ and $q_{\perp}$ (indicated in Fig. 1(d)) correspond to the long- and short-axis directions, respectively. The scattering intensity profiles obtained by averaging in the regions of $q_{//}$ and $q_{\perp}$ are shown in Fig. 1(f). The profile in the $q_{\perp}$ direction contains a peak at $q_{\perp} \approx 0.19\ \mathrm{nm}^{-1}$, which corresponds to an interparticle distance of $d \approx 33\ \mathrm{nm}$ in the short-axis direction. The profile in the $q_{//}$ direction contains two peaks at $q_{//} \approx 0.07\ \mathrm{nm}^{-1}$ and $0.19\ \mathrm{nm}^{-1}$. The peak at the lower value of q is considered to correspond to the interparticle distance in the long-axis

direction. The peak at the higher value of q is considered to originate from the interparticle distance in the short-axis direction in the minor domains with different orientations within the beam irradiation volume, since the peak position is almost identical to that observed for the peak in the $q_{\perp}$ direction.

Figure 2 shows the concentration dependence of the interparticle distance obtained from analysis of the SAXS images. For the isotropic phase with low concentration, interparticle distances of d = 49.0, 42.4, and 37.6 nm were obtained for ϕ_{HAp} = 3.8, 5.0, and 6.3 vol %, respectively. Thus, the interparticle distance clearly decreased with increasing concentration. In contrast, for the LC phase, the values of d in the short-axis direction were determined to be 34.8, 34.4, and 32.9 nm for ϕ_{HAp} = 6.5, 7.5, and 8.7 vol %, respectively, the variation of which is relatively small. Moreover, the values of d in the long-axis direction did not exhibit a clear dependence on the concentration, with d = 93.4, 87.7, and 93.2 nm for ϕ_{HAp} = 6.5, 7.5, and 8.7 vol %, respectively.

SAXS measurements were also performed for the long-term stationary samples. As with the short-term stationary samples, isotropic scattering images were obtained for the samples with ϕ_{HAp} = 3.8, 5.0, and 6.3 vol % and anisotropic images were obtained for the samples with ϕ_{HAp} = 6.5, 7.5, and 8.7 vol %. The interparticle distances obtained from the peak positions at each concentration are plotted in Fig. 2. For the isotropic phase, the values of d were found to be almost identical to those for the short-term stationary samples. In contrast, for the LC phase, the values of d in the short-axis direction were slightly lower than those for the short-term stationary samples for all of the measured concentrations. These results indicate the progress of particle packing in the short-axis direction in the LC phase. On the other hand, the values of d in the long-axis direction did not exhibit a clear dependence on the length of the stationary period. However, the error bars of d for the long axis in the LC phase show quite a clear difference depending on the length of the stationary period, which were obtained from the deviation of the data from the multiple measurements at the different positions. The error bars of d for the long axis in the LC phase for the short-term stationary samples were relatively large such as 1.4, 4.5 and 2.7 % for ϕ_{HAp} = 6.5, 7.5, and 8.7 vol %, respectively, whereas those for the long-term stationary samples were 0.5, 0.6 and 0.4 % for ϕ_{HAp} = 6.5, 7.5, and 8.7 vol %, respectively. Additionally, the error bars of d for the short axis in the LC phase for the short-term stationary samples were 0.3, 0.5 and 0.4 % for ϕ_{HAp} = 6.5, 7.5, and 8.7 vol %, respectively, whereas those for the long-term stationary samples were 0.2, 0.1 and 0.1 % for ϕ_{HAp} = 6.5, 7.5, and 8.7 vol %, respectively. These significant decrease of error bars of d with long-term stationary indicate the reduction of heterogeneity in the LC structure and the progress of particle packing in both of the short- and long- axis direction in the LC phase.

Moreover, the concentration dependence of *d* in the LC phase appears to become clear by the long-term stationary, namely the value of *d* decreases with increasing ϕ_{HAp} in both of the long- and short- axis direction. Discussing only the long-term stationary samples, the concentration dependence of *d* is larger in the long axis than in the short axis.

The packing behavior of colloidal particles may correlate to their orientation in the LC phase. When evaluating the degree of orientation, the azimuthal scattering intensity profile is conventionally discussed, the width of which should decrease with increasing degree of orientation.[32] Figure 3 shows the azimuthal scattering intensity profiles for the peak of $I(q)$ obtained at the high-q side and low-q side for the samples with ϕ_{HAp} = 6.5, 7.5, and 8.7 vol %. For the low-q side, the widths of the profiles hardly varied, as shown in Figs. 3(a)–(c). For the high-q side, the profile width became smaller after long-term storage for the samples with ϕ_{HAp} = 6.5 and 7.5 vol %, whereas it became larger for the sample with ϕ_{HAp} = 8.7 vol %, as shown in Figs. 3(d)–(f). Based on these results, it appears that the degree of orientation decreased for the sample with ϕ_{HAp} = 8.7 vol % and increased for the samples with ϕ_{HAp} = 6.5 and 7.5 vol %. However, it should be noted that the scattering images were obtained not from a single domain but from multiple domains within the irradiation volume ($\sim$100 μm × 200 μm × 2 mm) because the orientation was not deliberately induced but determined by gravity and the shape of the capillary tube. The anisotropy of the SAXS images reflects the orientation of the domains with a relatively large volume fraction. Thus, it cannot be definitively concluded that the degree of orientation decreased for the sample with ϕ_{HAp} = 8.7 vol % solely based on the increased width of the azimuthal intensity profile. Rather, considering that the interparticle distance in the short-axis direction decreased, there exists the possibility that the orientation in each domain was enhanced.

Dynamics in the LC phase

Figure 4 shows the measured time autocorrelation functions $g_2(q,t)$ at $q = 3.76 \times 10^{-2}\ \mathrm{nm}^{-1}$, which were obtained from the XPCS measurements, for the short-term stationary samples with ϕ_{HAp} = 6.5, 7.5, and 8.7 vol % in the LC phase. To evaluate the anisotropy of the dynamics, $g_2(q_{//},t)$ and $g_2(q_{\perp},t)$ are depicted separately. All of the $g_2(q,t)$ functions could be well fitted by a simple exponential function,

$$g_2(q,t) = A\exp(-2\Gamma t) + 1, \quad (2)$$

where A is the speckle contrast ($\sim$ 0.04) and Γ is the relaxation rate. Although $g_2(q_{//},t)$ and $g_2(q_{\perp},t)$ are plotted separately, the curves for the two functions were almost identical throughout the measured range of q values and no significant differences were observed. This is probably because the orientation of the particles was not enough to

observe the difference of the dynamics between in the long- and short-axis directions. Since no anisotropy of the dynamics was observed for the short-term stationary samples, the circularly averaged $g_2(q,t)$ data are analyzed in the following discussion for the short-term stationary samples.

Figure 5 shows the q dependence of Γ obtained by fitting analysis using Eq. (2). The plots reveal that Γ exhibited the fastest relaxation for the sample with ϕ_{HAp} = 6.5 vol %. The relaxation rate decreased with increasing concentration and Γ monotonically increased with q for all of the measured concentrations, although a downwardly convex hump was observed at approximately $q \approx 0.19$ nm^{-1} for the sample with ϕ_{HAp} = 8.7 vol %. Figure 6(a) shows the q-dependent diffusion coefficients $D(q)$, which were obtained using the formula $D(q) = \Gamma/q^2$. For the sample with ϕ_{HAp} = 8.7 vol %, $D(q)$ significantly decreased in the high-q region, and a minimum was observed at approximately $q \approx 0.2$ nm^{-1}. This minimum almost coincides with the position of the peak observed in the SAXS profile shown in Fig. 6(b). Since the peak in the SAXS profile represents the interparticle correlation of the nanorods in the short-axis direction, it can be considered that the decrease in $D(q)$ due to the interparticle correlation was successfully observed. In the intermediate-q region, slight decreases in $D(q)$ were observed at approximately $q \approx 0.07$ nm^{-1} for all of the measured concentrations. These are also considered the effects of interparticle correlation in the long-axis direction.

At all of the measured concentrations, $D(q)$ was constant in the low-q region ($q < 0.05$ nm^{-1}); that is, Γ was proportional to q^2 in the region of negligible interparticle correlation. Because of this, and because $g_2(q,t)$ could be fitted with a simple exponential function (Eq. (2)), the observed relaxation behavior is assumed to originate from simple Brownian motion of the colloidal particles. In the case of rod-like particles, the diffusion coefficient can be expressed as $D_0 = (D_{//} + 2D_{\perp})/3$, where $D_{//}$ and $D_{\perp}$ are the diffusion coefficients in the long- and short-axis directions, respectively.[33] In the present case, D_0 was estimated as 5.32×10^4, 2.94×10^4, and 0.94×10^4 nm^2 s^{-1} for the samples with ϕ_{HAp} = 6.5, 7.5, and 8.7 vol %, respectively.

Next, the XPCS data obtained for the long-term storage samples are discussed. Figure 7 shows $g_2(q_{//},t)$ and $g_2(q_{\perp},t)$ for the long-term stationary samples at $q = 4.76 \times 10^{-2}$ nm^{-1}. For all of the measured concentrations, $g_2(q_{//},t)$ exhibited faster relaxation than $g_2(q_{\perp},t)$, which indicates the occurrence of faster dynamics in the long-axis direction than in the short-axis direction. Although satisfactory fitting of $g_2(q_{//},t)$ and $g_2(q_{\perp},t)$ could not be obtained using Eq. (2), the two functions could be well fitted using the following stretched exponential function:

$$g_2(q,t) = A\exp\left[-2(\Gamma t)^{\gamma}\right] + 1, \quad (3)$$

where the averaged stretching value γ was 0.7, 0.6, and 0.4 for the samples with ϕ_{HAp} = 6.5, 7.5, and 8.7 vol %, respectively. The finding that $g_2(q,t)$ could be fitted using Eq. (3) but not Eq. (2) suggests that the observed dynamical behavior is no longer simple Brownian motion. It is considered that a change in the packing or orientation of the particles upon long-term storage may have affected the dynamical behavior of the particles.

Figure 8 shows the q dependence of Γ obtained by fitting analysis using Eq. (3). The plots reveal that the Γ obtained from $q_{//}$ was faster than the Γ obtained from $q_{\perp}$ at all of the measured concentrations and throughout all of the measured range of q. Figure 9 shows the behavior of $D(q)$ calculated using Γ/q^2. The plots reveal that $D(q_{//}) > D(q_{\perp})$, and a local minimum due to the interparticle correlation was observed at approximately $q \approx 0.2$ nm^{-1} for the sample with ϕ_{HAp} = 8.7 vol %. In previous studies, the diffusion coefficients were separately evaluated for the long- and short-axis directions of the nematic phase. [9,10,34,35] Compared with these previous results, the difference between $D(q_{//})$ and $D(q_{\perp})$ obtained herein is much smaller. This may be because the dynamics observed in this study originated not from a single domain but from the multiple domains present within the irradiation volume (~20 μm × 20 μm × 2 mm).

Compared with $D(q)$ obtained from the short-term storage samples, slower dynamics were observed for the long-term storage samples. The degree of slowing down was dependent on the concentration. Although the change in $D(q)$ was relatively small for the sample with ϕ_{HAp} = 6.5 vol %, $D(q)$ reduced by about half for the sample with ϕ_{HAp} = 7.5 vol %. Moreover, for the sample with ϕ_{HAp} = 8.7 vol %, $D(q)$ became an order of magnitude smaller compared with the short-term storage sample. This phenomenon of slower dynamics over time has been previously reported for LC polymer melts by Gochanour and Weinberg.[36] They investigated the variation in rheological properties as a function of time at constant temperature and found that the viscosity increased with time. Although a coherent explanation for this phenomenon was not provided, one possibility noted by the authors is that the crystalline structure became larger or more perfect over time.

Considering that the difference in $D(q)$ between the short-term storage samples and long-term storage samples increases with increasing ϕ_{HAp}, it can be assumed that cooperative motion occurs in addition to the individual diffusive motion. From this perspective, it is possible to rationalize the behavior of $D(q)$ at high q for the sample with ϕ_{HAp} = 8.7 vol %, which was higher than at low q. It can be assumed that $D(q)$ at low q is sensitive to the cooperative motion, whereas $D(q)$ at high q reflects the individual dynamics of the particles and exhibits fast behavior.

Conclusions

The static structure and dynamics of aqueous HAp colloids, which undergo a phase transition between the isotropic and LC phases above a certain concentration, were investigated by SAXS and XPCS. We performed measurements for short-term stationary samples and long-term storage samples and examined the changes observed in the samples depending on the storage period.

In the studies of the static structure, the concentration dependence of the interparticle distance was evaluated. For the isotropic phase, the interparticle distance noticeably decreased with increasing particle concentration. In contrast, for the LC phase, the concentration dependence of the interparticle distance was relatively minor in the short-axis direction and no clear trend was observed in the long-axis direction. After long-term storage, we observed a decrease in the interparticle distance in the short-axis direction, which implies an improvement in the colloidal packing in the short-axis direction.

In the studies of the dynamics, for the short-term storage samples, simple Brownian motion was observed in the low-q region, and the diffusion coefficients were estimated as constant values at each concentration. In contrast, in the high-q region where the interparticle correlation is considerable, decreases in the diffusion coefficients were observed. Thus, we obtained the diffusion coefficients depending on q. For the long-term storage samples, we observed anisotropic dynamics, which implies an enhanced degree of orientation in each domain after long-term storage. Moreover, we observed slower dynamics, the degree of which was dependent on the concentration. This is also assumed to be attributable to the enhancement of the colloidal packing and degree of orientation.

In this study, the anisotropy of the dynamics was observed for the particle orientation induced by gravity or the cell shape. This degree of orientation was not sufficient to permit a quantitative discussion of the individual diffusion coefficients in the short- and long-axis directions. It has been reported that the orientation of HAp nanorods can be controlled using an external magnetic field.[6] The utilization of such a method to forcibly orient the particles would be expected to allow a more sophisticated discussion of the degree of orientation and q-dependent diffusion coefficient.

Acknowledgements

The XPCS experiments at beamline BL29XUL were performed under the approval of RIKEN (Proposal Nos. 20170026 and 20180027). The work of T.H., S.F., and T.N. was partially supported by the ImPACT Program of the Council for Science, Technology and Innovation (Cabinet Office, Government of Japan). T.H. acknowledges JST,

PRESTO, for funding the project “Molecular technology and creation of new functions” and a JSPS Grant-in-Aid for Scientific Research (C) (18K05226). T.K. acknowledges JSPS KAKENHI Grant Number JP15H02179. The work of M.N. was partially supported by JSPS KAKENHI Grant Number JP17J09259.

References

1. L. C. Palmer, C. J. Newcomb, S. R. Kaltz, E. D. Spoerke and S. I. Stupp, *Chem. Rev.*, 2008, **108**, 4754-4783.

2. U. G. K. Wegst, H. Bai, E. Saiz, A. P. Tomsia and R. O. Ritchie, *Nat. Mater.*, 2014, **14**, 23-36.

3. T. Kato, T. Sakamoto and T. Nishimura, *MRS Bulletin*, 2011, **35**, 127-132.

4. A. Arakaki, K. Shimizu, M. Oda, T. Sakamoto, T. Nishimura and T. Kato, *Org Biomol Chem*, 2015, **13**, 974-989.

5. F. Nudelman and N. A. Sommerdijk, *Angew. Chem. Int. Ed.*, 2012, **51**, 6582-6596.

6. M. Nakayama, S. Kajiyama, A. Kumamoto, T. Nishimura, Y. Ikuhara, M. Yamato and T. Kato, *Nat Commun*, 2018, **9**, 568.

7. M. Doi and S. F. Edwards, *The Theory of Polymer Dynamics*, Oxford University Press, 1986.

8. Z. Dogic and S. Fraden, *Current Opinion in Colloid & Interface Science*, 2006, **11**, 47-55.

9. M. P. Lettinga, E. Barry and Z. Dogic, *Europhys Lett*, 2005, **71**, 692-698.

10. M. P. Lettinga, J. K. G. Dhont, Z. Zhang, S. Messlinger and G. Gompper, *Soft*

Matter, 2010, **6**, 4556.

11. E. Pouget, E. Grelet and M. P. Lettinga, *Phys Rev E Stat Nonlin Soft Matter Phys*, 2011, **84**, 041704.
12. R. Pecora, *The Journal of Chemical Physics*, 1968, **48**, 4126-4128.
13. D. Lehner, H. Lindner and O. Glatter, *Langmuir*, 2000, **16**, 1689-1695.
14. A. D. Levin, E. A. Shmytkova and B. N. Khlebtsov, *The Journal of Physical Chemistry C*, 2017, **121**, 3070-3077.
15. I. Martchenko, H. Dietsch, C. Moitzi and P. Schurtenberger, *J Phys Chem B*, 2011, **115**, 14838-14845.
16. M. P. Allen, *Phys Rev Lett*, 1990, **65**, 2881-2884.
17. S. Hess, D. Frenkel and M. P. Allen, *Molecular Physics*, 1991, **74**, 765-774.
18. H. Lowen, *Physical Review E*, 1999, **59**, 1989-1995.
19. A. Patti and A. Cuetos, *Phys Rev E Stat Nonlin Soft Matter Phys*, 2012, **86**, 011403.
20. S. Jabbari-Farouji and E. Trizac, *J Chem Phys*, 2012, **137**, 054107.
21. A. Cuetos and A. Patti, *Phys Rev E Stat Nonlin Soft Matter Phys*, 2015, **92**, 022302.
22. J. C. Brown, P. N. Pusey, J. W. Goodwin and R. H. Ottewill, *J Phys a-Math Gen*,

1975, **8**, 664-682.

23. C. BEENAKKER and P. MAZUR, *Physica A*, 1984, **126**, 349.

24. C. G. de Kruif, E. M. F. van Iersel, A. Vrij and W. B. Russel, *The Journal of Chemical Physics*, 1985, **83**, 4717-4725.

25. P. N. Segrè, O. P. Behrend and P. N. Pusey, *Physical Review E*, 1995, **52**, 5070-5083.

26. O. K. C. Tsui and S. G. J. Mochrie, *Physical Review E*, 1998, **57**, 2030-2034.

27. L. B. Lurio, D. Lumma, A. R. Sandy, M. A. Borthwick, P. Falus, S. G. Mochrie, J. F. Pelletier, M. Sutton, L. Regan, A. Malik and G. B. Stephenson, *Phys Rev Lett*, 2000, **84**, 785-788.

28. D. O. Riese, G. H. Wegdam, W. L. Vos, R. Sprik, D. Fenistein, J. H. Bongaerts and G. Grubel, *Phys Rev Lett*, 2000, **85**, 5460-5463.

29. P. Holmqvist, V. Meester, F. Westermeier and D. Kleshchanok, *J Chem Phys*, 2013, **139**, 084905.

30. J. Wagner, C. Markert, B. Fischer and L. Muller, *Phys Rev Lett*, 2013, **110**, 048301.

31. K. Tamasaku, Y. Tanaka, M. Yabashi, H. Yamazaki, N. Kawamura, M. Suzuki, and T. Ishikawa, *Nucl Instrum Meth A*, 2001, **467**, 686-689.

32. N. S. Murthy, J. R. Knox and E. T. Samulski, *Journal of Chemical Physics*, 1976, **65**, 4835-4839.

33. B. J. Berne and R. Pecora, *Dynamic light scattering : with applications to chemistry, biology, and physics*, Wiley, New York, 1976.

34. S. V. Dvinskikh and I. Furó, *The Journal of Chemical Physics*, 2001, **115**, 1946-1950.

35. S. V. Dvinskikh, I. Furo, H. Zimmermann and A. Maliniak, *Phys Rev E Stat Nonlin Soft Matter Phys*, 2002, **65**, 061701.

36. C. R. Gochanour and M. Weinberg, *Journal of Rheology*, 1986, **30**, 101-124.

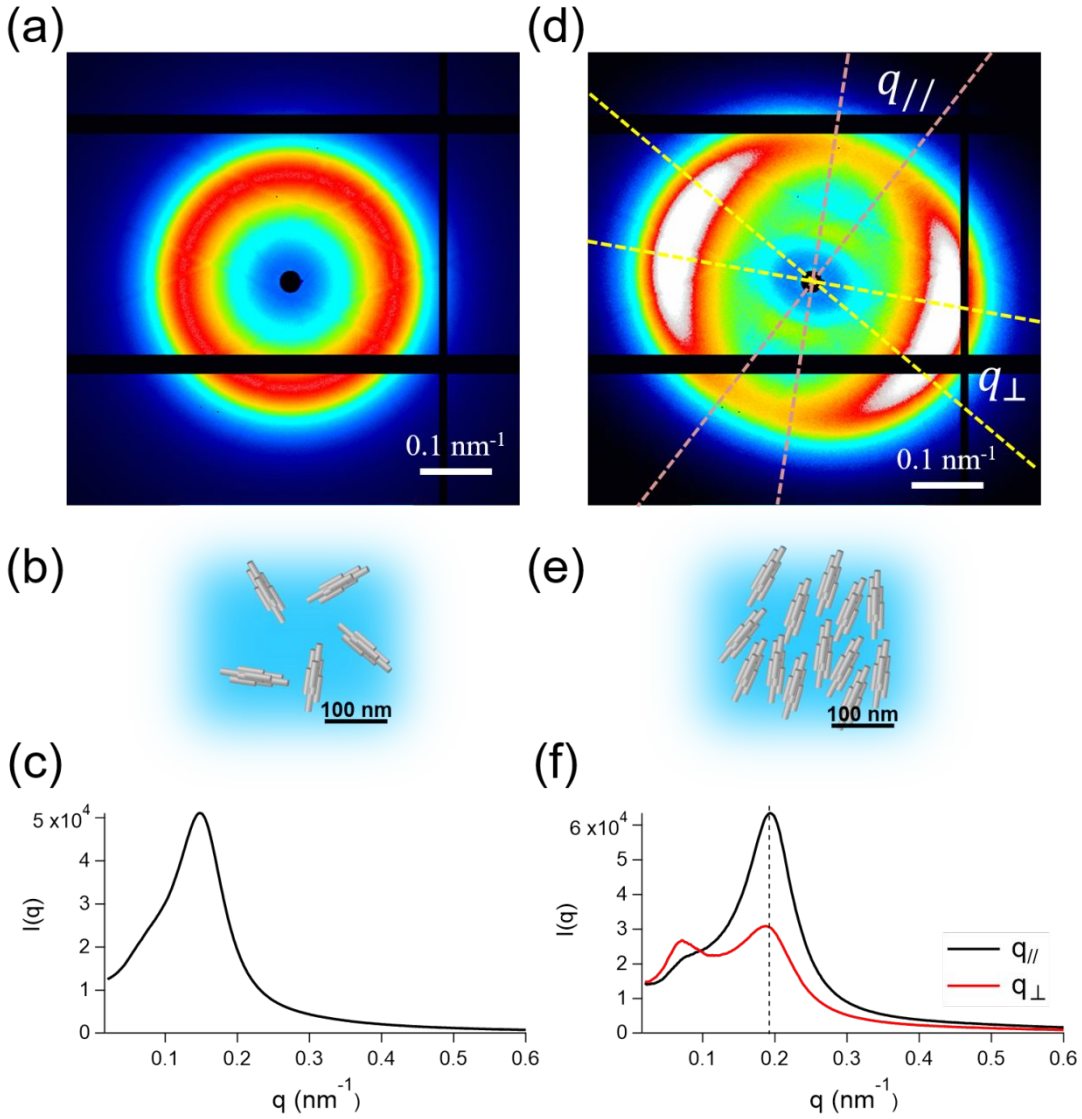

Fig. 1. Representative scattering data obtained for the short-term stationary samples. (a) Scattering image, (b) schematic illustration of HAp nanorods in aqueous colloidal dispersion and (c) circularly averaged intensity profile $I(q)$ for the sample with $\phi_{\mathrm{HAp}} = 5.0$ vol %. (d) Scattering image, (e) schematic illustration of HAp nanorods in aqueous colloidal dispersion and (f) circularly averaged intensity profile $I(q)$ for the sample with $\phi_{\mathrm{HAp}} = 8.7$ vol %. The black and red lines in (f) were obtained by averaging in the regions of $q_{//}$ and $q_{\perp}$ shown in (d), respectively.

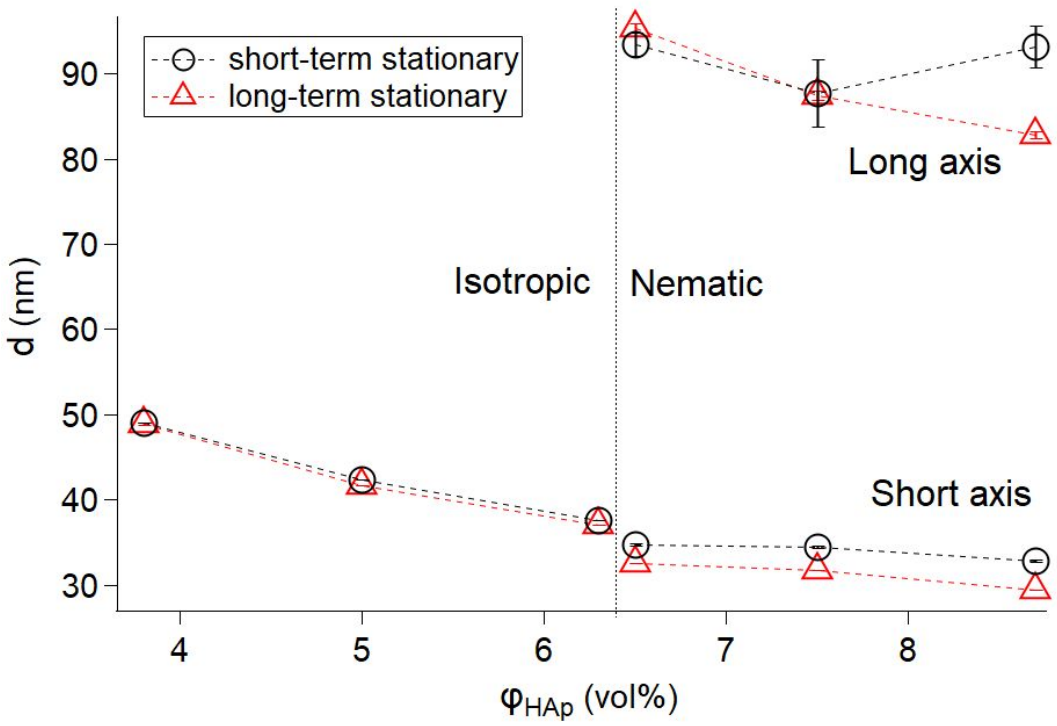

Fig. 2. Concentration dependence of the interparticle distance obtained from the SAXS measurements. The black circles and red triangles indicate the data for the short-term stationary (15 days after sealing) and long-term stationary (185 days after sealing) samples, respectively.

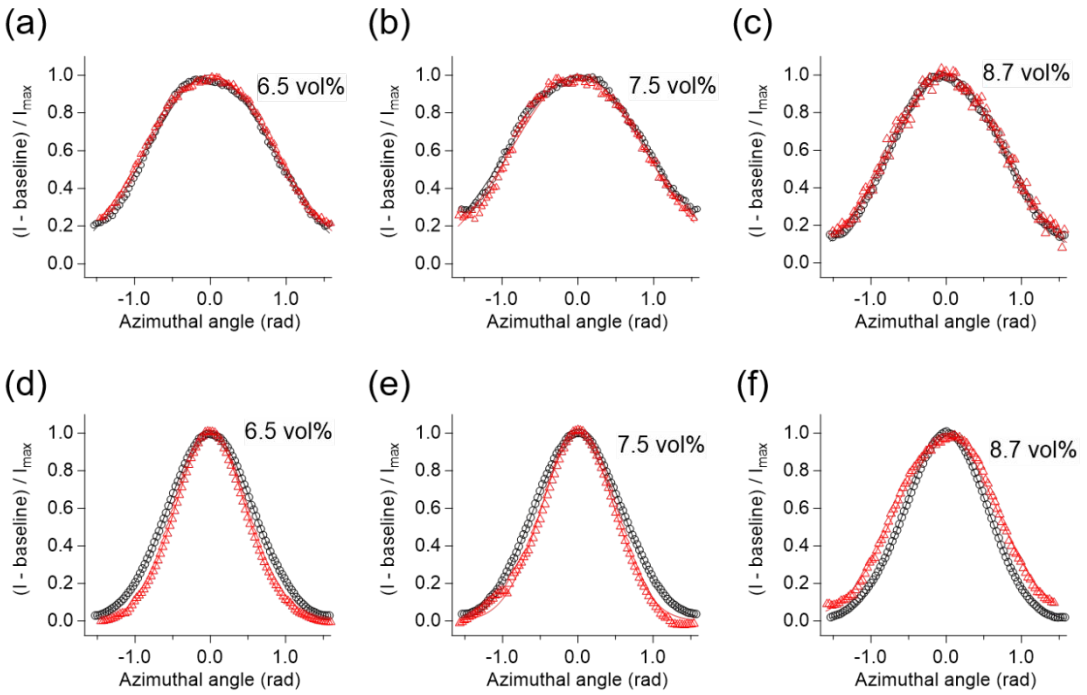

Fig. 3. Azimuthal scattering intensity profiles for the peak of $I(q)$ obtained at (a)–(c) the low-q side and (d)–(f) the high-q side for the samples with ϕ_{HAp} = 6.5, 7.5, and 8.7 vol %. The black circles and red triangles indicate the data for the short-term stationary and long-term stationary samples, respectively.

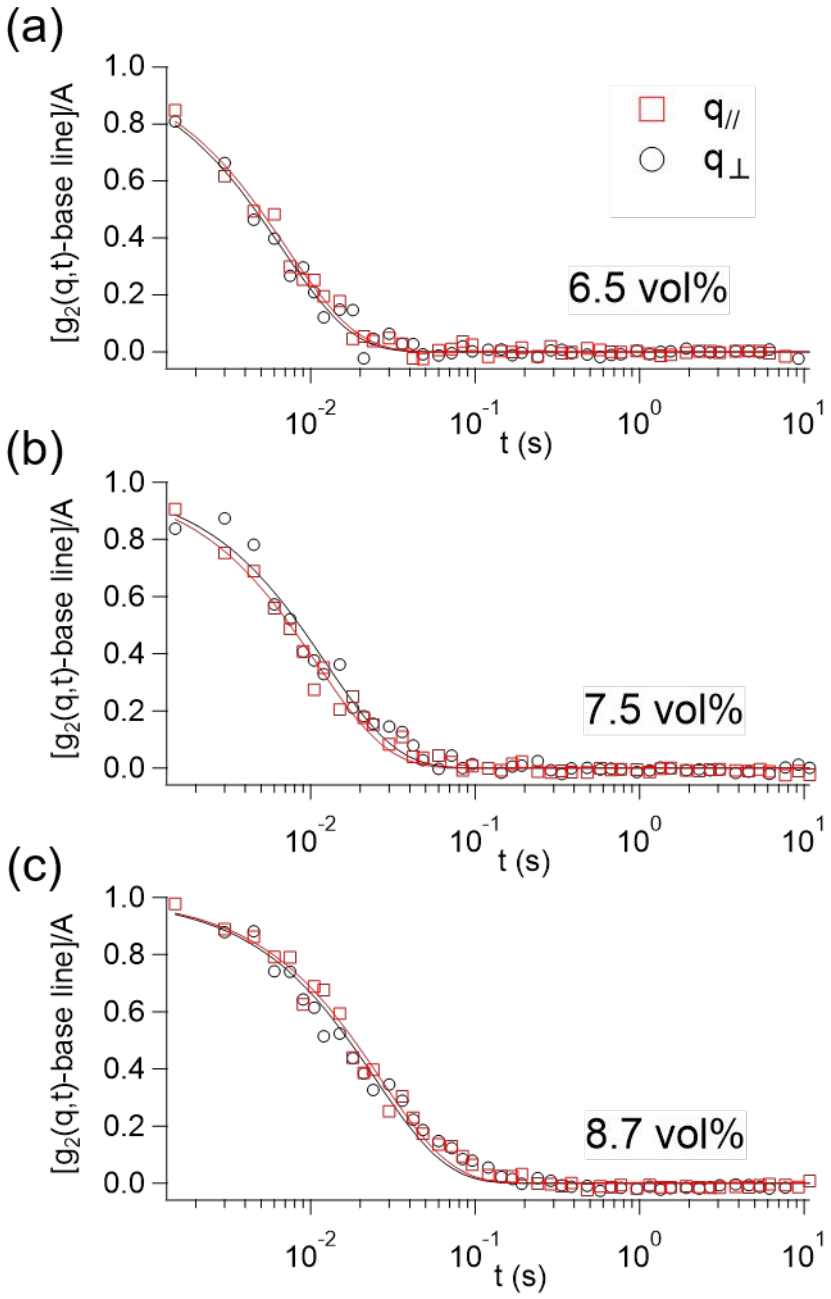

Fig. 4. Measured time autocorrelation functions $g_2(q,t)$ at $q = 3.76 \times 10^{-2}\,\mathrm{nm}^{-1}$ obtained from the XPCS measurements for the short-term stationary samples with ϕ_{HAp} = (a) 6.5, (b) 7.5, and (c) 8.7 vol %. The red squares and black circles indicate the data for $g_2(q_{//},t)$ and $g_2(q_{\perp},t)$, respectively. The solid lines represent the fitting curves obtained using Eq. (2).

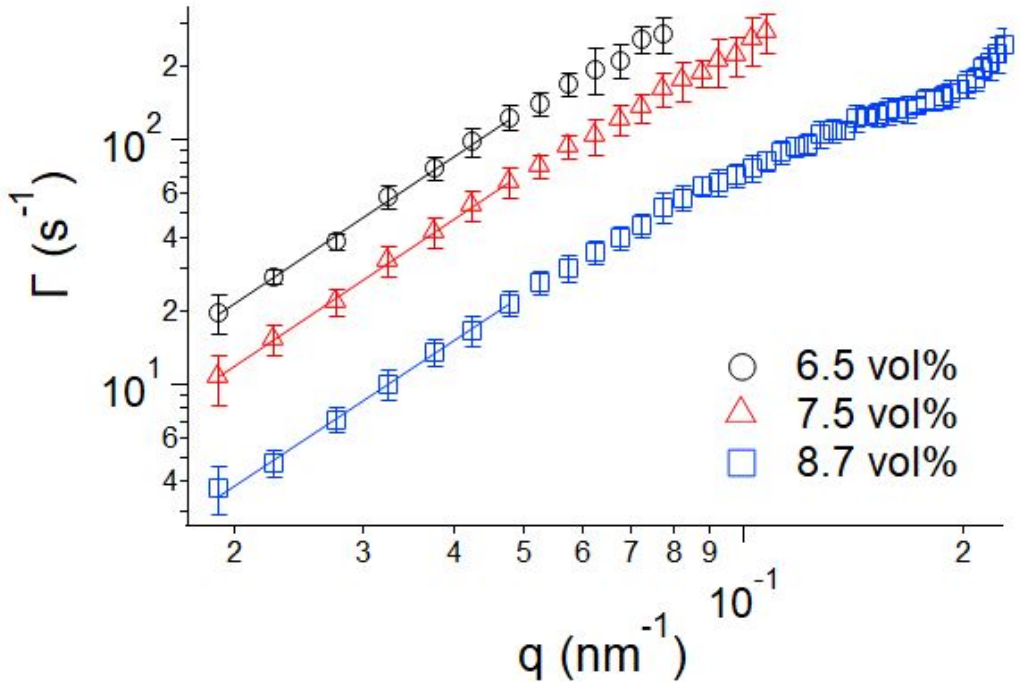

Fig. 5. q dependence of Γ obtained by fitting analysis using Eq. (2) for the short-term stationary samples with ϕ_{HAp} = 6.5, 7.5, and 8.7 vol %. The solid lines represent the fitting lines proportional to q^2 at $q < 0.05$ nm^{-1}.

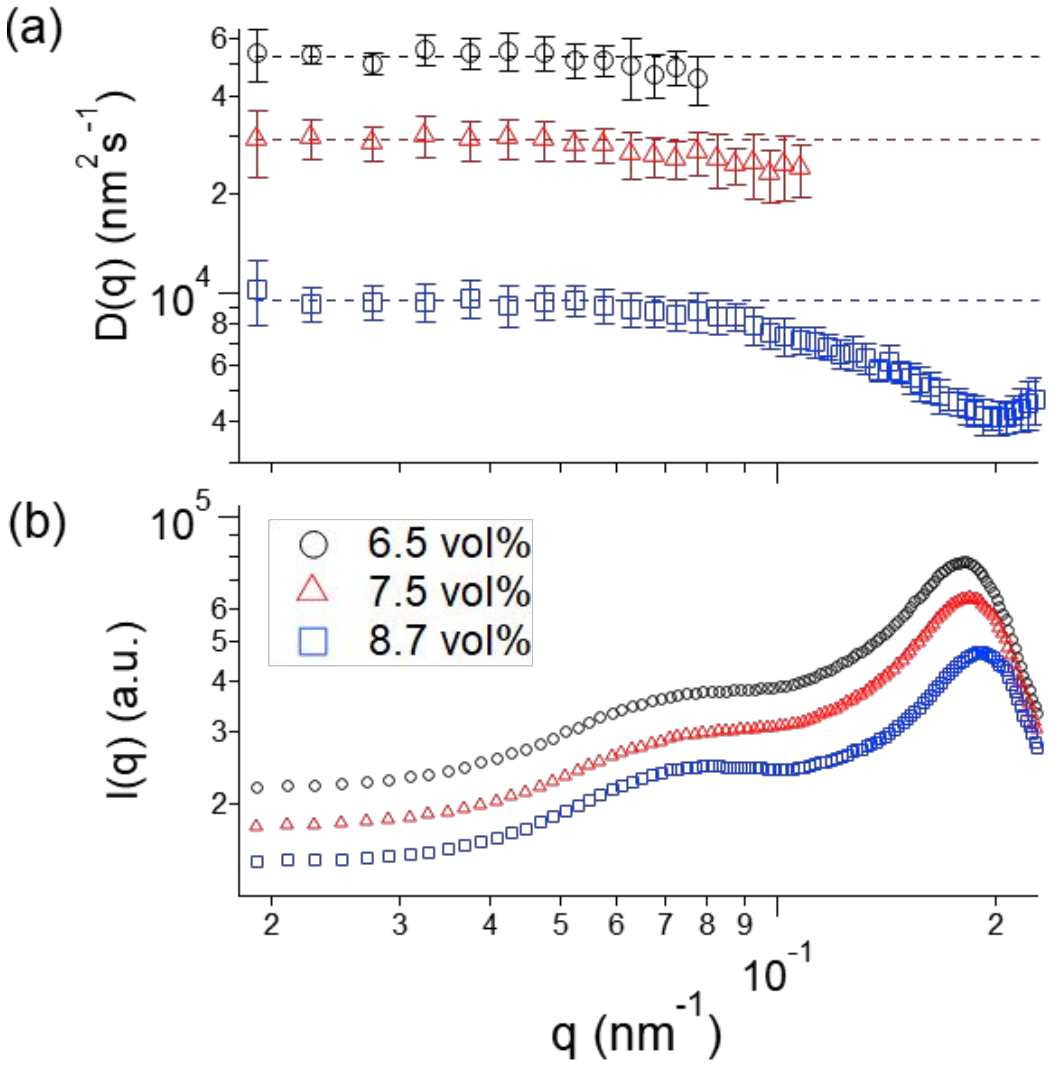

Fig. 6. (a) q-dependent diffusion coefficients $D(q)$, obtained by dividing Γ by q^2 for the short-term stationary samples with ϕ_{HAp} = 6.5, 7.5, and 8.7 vol %. (b) Scattering intensity profiles obtained from the circularly averaged SAXS images for the samples with ϕ_{HAp} = 6.5, 7.5, and 8.7 vol %.

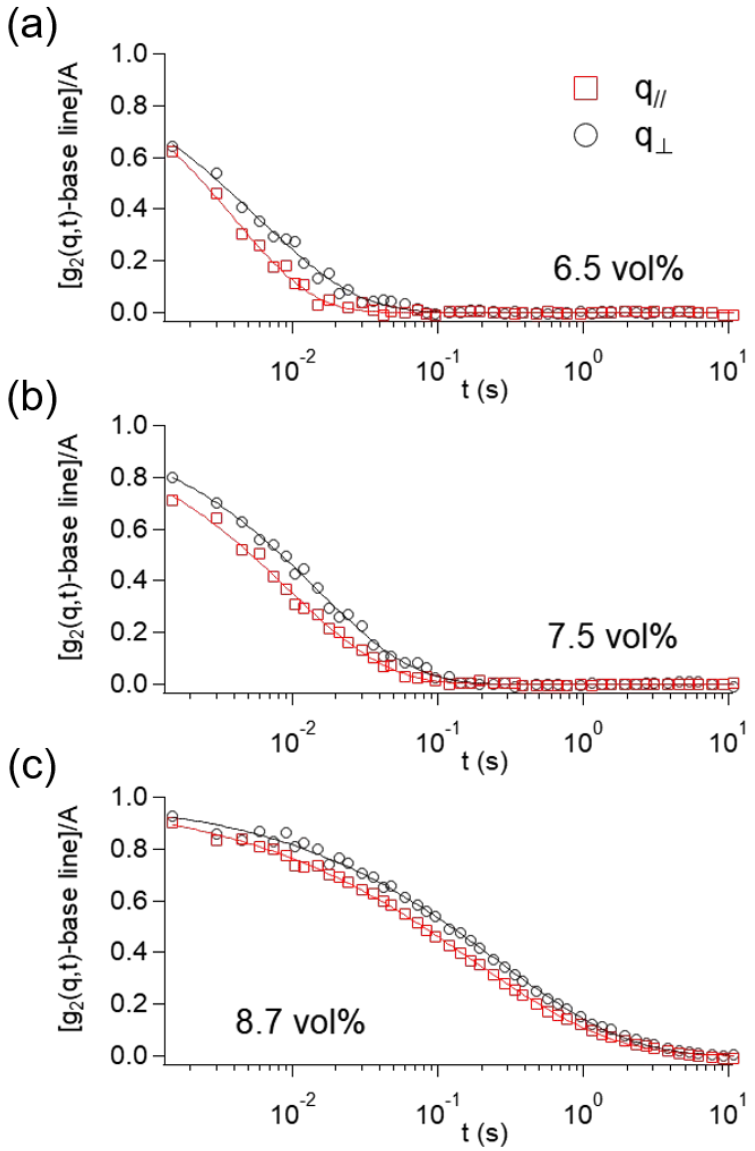

Fig. 7. Measured time autocorrelation functions $g_2(q,t)$ at $q = 4.76 \times 10^{-2}\,\mathrm{nm}^{-1}$ obtained from the XPCS measurements for the long-term stationary samples with ϕ_{HAp} = (a) 6.5, (b) 7.5, and (c) 8.7 vol %. The red squares and black circles indicate the data for $g_2(q_{//},t)$ and $g_2(q_{\perp},t)$, respectively. The solid lines represent the fitting curves obtained using Eq. (3).

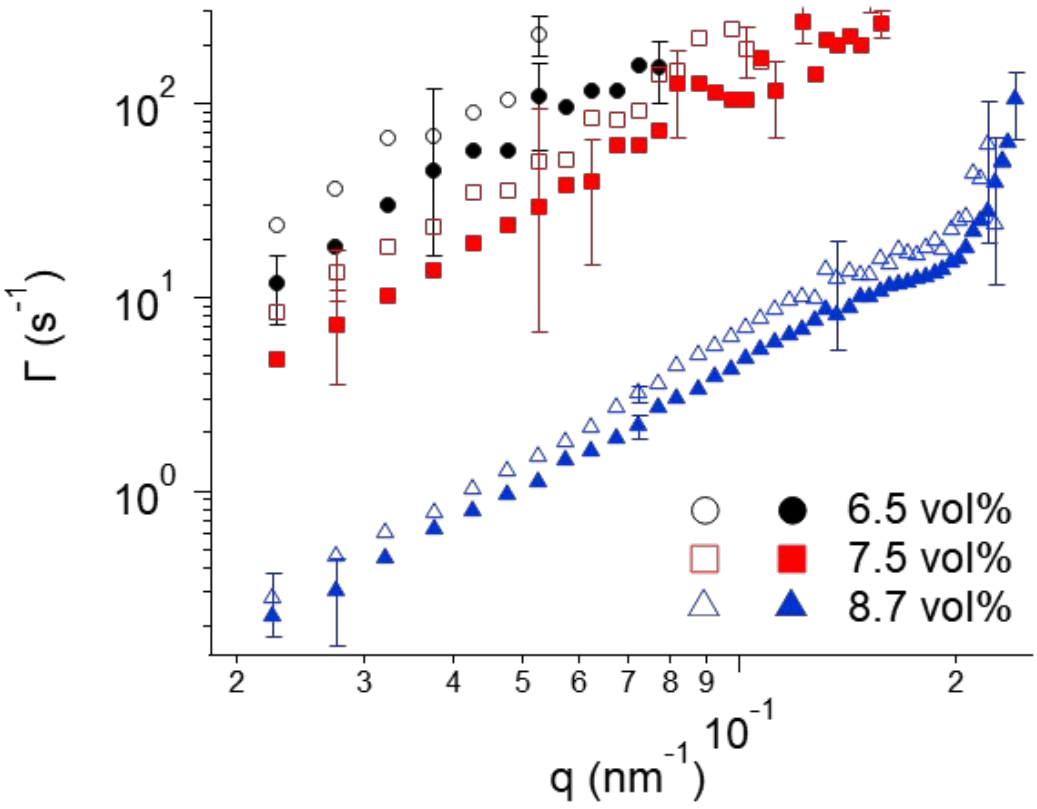

Fig. 8. q dependence of Γ obtained by fitting analysis using Eq. (3) for the long-term stationary samples with ϕ_{HAp} = 6.5, 7.5, and 8.7 vol %. The open and closed symbols correspond to the Γ obtained from $q_{//}$ and $q_{\perp}$, respectively. For clarity, only typical error bars are depicted.

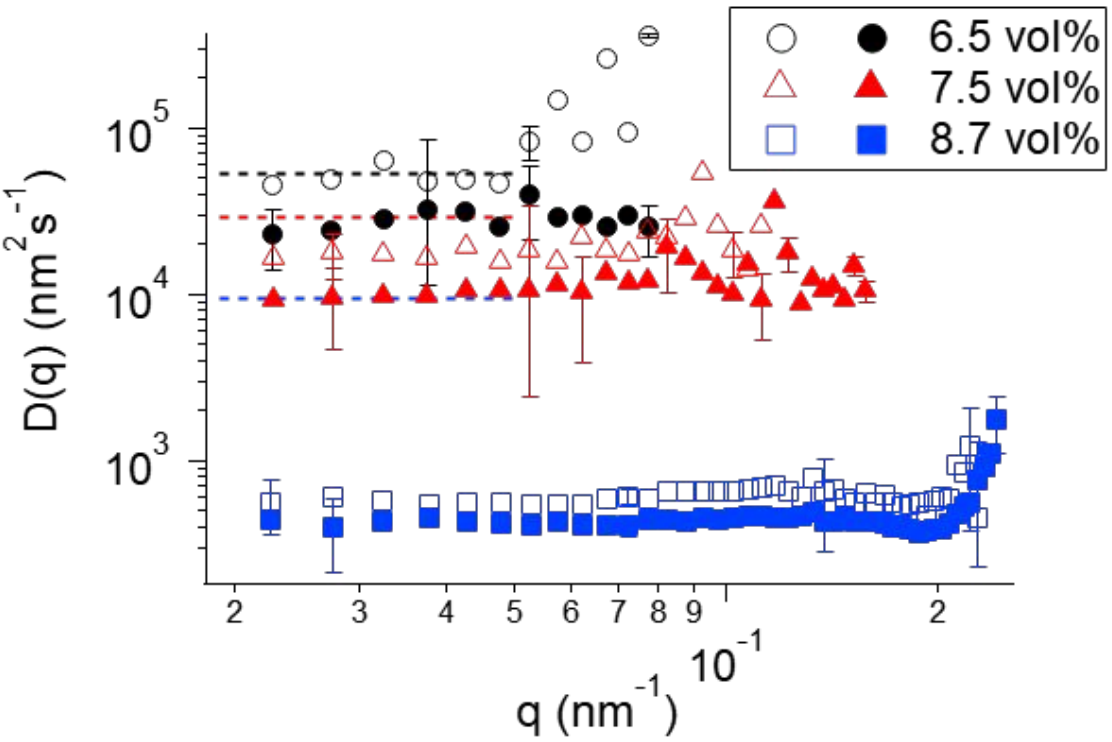

Fig. 9. Variation of $D(q)$, obtained by dividing Γ by q^2, for the long-term stationary samples with ϕ_{HAp} = 6.5, 7.5, and 8.7 vol %. The open and closed symbols correspond to the $D(q)$ obtained from $q_{//}$ and $q_{\perp}$, respectively. For clarity, only typical error bars are depicted. The dashed lines indicate the diffusion coefficients for the short-term stationary samples at $q < 0.05$ nm^{-1}.